Predictability of Rayleigh-Number and Continental-Growth Evolution of a Dynamic Model of the Earth's Mantle

Uwe Walzer and Roland Hendel

Abstract We compute a model of thermal and chemical evolution of the Earth's mantle by numerically solving the balance equations of mass, momentum, energy, angular momentum and of four sums of the number of atoms of the pairs ^{238}U-^{206}Pb, ^{235}U-^{207}Pb, ^{232}Th-^{208}Pb, and ^{40}K-^{40}Ar. We derive marble-cake distributions of the principal geochemical reservoirs and show that these reservoirs can separately exist even in a present-day mantle in spite of 4500 Ma of thermal convection. We arrive at plausible present-day distributions of continents and oceans although we did not prescribe number, size, form, and distribution of continents. The focus of this paper is the question of predictable and stochastic portions of the phenomena. Although the convective flow patterns and the chemical differentiation of oceanic plateaus are coupled, the evolution of time-dependent Rayleigh number, Ra_I, is relatively well predictable and the stochastic parts of the $Ra_I(t)$-curves are small. Regarding the juvenile growth rates of the total mass of the continents, predictions are possible only in the first epoch of the evolution. Later on, the distribution of the continental-growth episodes is increasingly stochastic. Independently of the varying individual runs, our model shows that the total mass of the present-day continents is *not* generated in a single process at the beginning of the thermal evolution of the Earth but in episodically distributed processes in the course of geological time. This is in accord with observation. Section 4 presents results on scalability and performance.

1 Introduction: Generation of Continents

The problem of the development of continents is very complex [5]. Condie [8] shows that the total volume of continents did *not* originate as a whole at the beginning of the Earth's thermal evolution but by repeated differentiation cycles. Only about one half of the present total volume was produced by chemical differentiation until the end of the Archean, 2500 Ma ago. Kramers and Tolstikhin [16] conclude from the U-Th-Pb isotope system, Nagler and Kramers [18] deduce from the neodymium system that less than 10% of the present mass of the continental crust have existed 4400 Ma ago. Fisher and Schmincke [10] estimate that *today* about 62 vol.% of the

U. Walzer · R. Hendel

Institut für Geowissenschaften, Friedrich-Schiller-Universität, Burgweg 11, 07749 Jena, Germany

e-mail: u.walzer@uni-jena.de; roland.hendel@uni-jena.de

general crustal growth takes place at divergent plate boundaries, about 24 vol.% at convergent plate boundaries and only about 12 vol.% as ocean island and plateau basalts by plumes. The differentiation of continental material via oceanic plateaus complementary creates a depleted part of the mantle beneath the lithosphere. Observational evidence suggests that the contribution of oceanic plateaus to continental growth seems to have been considerably larger than that of the mid-ocean ridge basalt (MORB) of the divergent plate boundaries in the bulk of *earlier* geological epochs compared to the present [19]. In epochs of *large* continental growth, the contribution of plateau basalts were considerably larger than today, and these mantle-differentiation events had an episodic temporal distribution [7]. There are clearly investigated examples of large oceanic plateaus which have been accreted to the Americas [3, 15]. Abbott et al. [1] and Albarède [2] concluded that the accretion of oceanic-plateau basalts to the continental crust (CC) is, considering the whole time span of Earth's history, the dominant process and that basaltic crust with more than 25 km thickness cannot be subducted. But there are also some other mechanisms which contribute to continental growth [9]. Our numerical model of the dynamics of continental growth [23] is based on geochemical observations and its generalization given by Hofmann [13, 14]. Incompatible elements have large s-, p-, d-, and f-radii. Therefore, these elements do not fit well into the silicate lattices of the mantle and Rb, Pb, U, Th, K, La etc. are enriched in partial melts. These melts rise and form the oceanic plateaus leaving behind the depleted MORB mantle (DMM). So, DMM is depleted in comparison to the primitive mantle (PM). In this way, the three main reservoirs (CC, DMM, PM) of the silicate shell of the Earth are generated. They have different abundances of the dominating heat-producing elements, U, Th, and K, that drive the solid-state convection mainly by heating from within. The further chemical differentiation of DMM at the mid-oceanic ridges into a basaltic oceanic crust and the harzburgitic and lherzolitic layers of the oceanic lithospheric mantle has been neglected up to now. This introduction is strongly simplified. Walzer et al. [25] discuss the mantle chemistry, the mantle processes, and their translation into our model in detail.

2 Model and First Results

Walzer et al. [25] describe the derivation of the governing equations of our convection-differentiation model. Walzer and Hendel [23] present a numerical model in which 3-D compressional spherical-shell convection, thermal evolution of the Earth, chemical differentiation of plateau basalts and continental growth are integrated. The model equations guarantee the conservation of mass, momentum, energy, angular momentum, and of four sums of the number of atoms of the pairs ^{238}U-^{206}Pb, ^{235}U-^{207}Pb, ^{232}Th-^{208}Pb, and ^{40}K-^{40}Ar. Nevertheless, the present companion paper presents exclusively additional, unpublished material.

We express the chemistry of incompatible elements of the three reservoirs (CC, DMM, PM) by tracers. These tracers are entrained in the convective currents. Since

93 internal heating and buoyancy depend on the abundances of radionuclides, the trac-
94 ers actively influence the convection. As the *current* geochemical reservoir models
95 [4, 14, 22, 26] do, our numerical model allows stirring and mixture of the reservoirs.
96 If the temperature, T, approaches to the melting temperature, T_m, in a sufficiently
97 large region of the modeled spherical shell then CC-tracers are produced from for-
98 mer PM-tracers. The CC-tracers rise and form the oceanic plateaus at the surface.
99 This mimics the plume volcanism. Walzer et al. [24] modeled the self-consistent
100 generation of oceanic lithospheric plates with individual, different angular veloc-
101 ity vectors for the different plates on the spherical shell. Such oceanic lithospheric
102 plates are also generated in the present convection-differentiation model. They carry
103 the oceanic plateaus like a conveyor belt. If the plateaus touch a continent they are
104 joined with it in such way that the continent and the plateau have a future com-
105 mon angular velocity. In this way, the continent has been enlarged by accretion.
106 Continents are unsinkable but else they are freely driven by the convection without
107 further constraints. No restrictions are imposed regarding number, form, size and
108 distribution of continents.
109 The former PM-tracers of the differentiation region are left behind as DMM-
110 tracers in the upper mantle. So, DMM is growing whereas PM is shrinking. After
111 Hofmann [14], between 30 and 80% of the mantle are depleted (DMM) for the
112 present day, according to Bennett [4] 30 to 60%. Figure 1 displays that our model
113 fulfills these requirements. The presented equatorial section shows a marble-cake
114 distribution of depleted portions of the mantle (yellow) and enriched mantle portions
115 (orange). Everywhere immediately beneath the lithosphere, we obtain a depleted
116 mantle in accord with observations. The continents are shown in red color. We used
117 the viscosity profile of Walzer et al. [24]. In this profile, strong viscosity gradients
118 are induced by discontinuities of activation volume and activation energy at the
119 mineral phase boundaries of the mantle. The phase boundaries also generate the
120 observed jumps of seismic velocities. In spite of this viscosity profile, Fig. 1 and
121 lots of similar results do *not* show chemical layering. Only the upper part of the
122 asthenosphere is mainly composed of DMM since the differentiation occurs in that
123 region.
124 The growth of the total mass of the continents is not uniformly but episodically
125 distributed as a function of time. Cf. Fig. 2, second panel. This is in accord with ob-
126 servation [8]. Figure 1 shows that in spite of mantle convection, enduring 4500 Ma,
127 we do not observe a total homogenization of the mantle but the preservation of de-
128 pleted, "yellow" slabs and pancake-like regions and, simultaneously, of enriched
129 regions. So, this model is able to explain the present-day existence of geometri-
130 cally distinct geochemical reservoirs in spite of convection. However, in general,
131 the yellow-orange boundary does not correspond to a discontinuity of the abundance
132 distributions. The nonexistence of a present-day total homogenization is primarily
133 induced by the viscosity profile and to a minor degree by the phase boundary dis-
134 placements due to rising and sinking material. The laterally averaged surface heat
135 flow, qob, decreases slowly as a function of time and shows some variations. Cf.
136 Fig. 2, first panel. For the present day, it arrives nearly at the observed value. It is
137 remarkable that the decrease of qob is much less pronounced than in usual parame-
138 terized models [21].
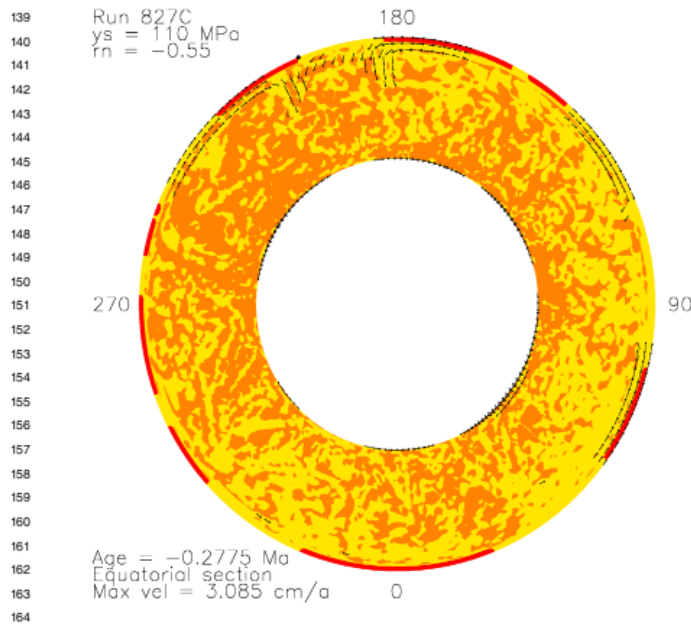
Fig. 1 The result of chemical evolution of the silicate spherical shell of the Earth, using the parameters $\sigma_y = 110$ MPa and $r_n = -0.5$ (cf. Sect. 2), for the present day. We assume a modernized reservoir theory (cf. [4, 14, 23]). Strongly depleted portions of the mantle which include more than 50% DMM are displayed by *yellow areas*. Enriched portions of the mantle with less than 50% DMM are *orange-colored*. In general, the *yellow-orange* boundary does *not* correspond to a discontinuity of the abundances of incompatible elements. The cross sections through the continents are *red*

This behavior is induced by the implicit assumption that water dependence of viscosity, dehydration near the surface and chemical layering of the oceanic lithosphere are more important for the lithospheric viscosity than its temperature dependence. About 50 ppm hydrogen reduces the viscosity of olivine by a factor of 30–100 [12, 17]. Essentially, we assume Newtonian solid-state creep for the mantle. The shear viscosity, η, is given by

$$\eta(r, \theta, \phi, t) = 10^{r_n} \cdot \frac{\exp(c\overline{T_m / T_{av}})}{\exp(c\overline{T_m / T_{st}})} \cdot \eta_3(r) \cdot \exp\left[c_t \cdot T_m \left(\frac{1}{T} - \frac{1}{T_{av}}\right)\right] \quad (1)$$

where r is the radius, θ the colatitude, ϕ the longitude, t the time, r_n the viscosity-level parameter, T_m the melting temperature, T_{av} the laterally averaged temperature,

Case 827C
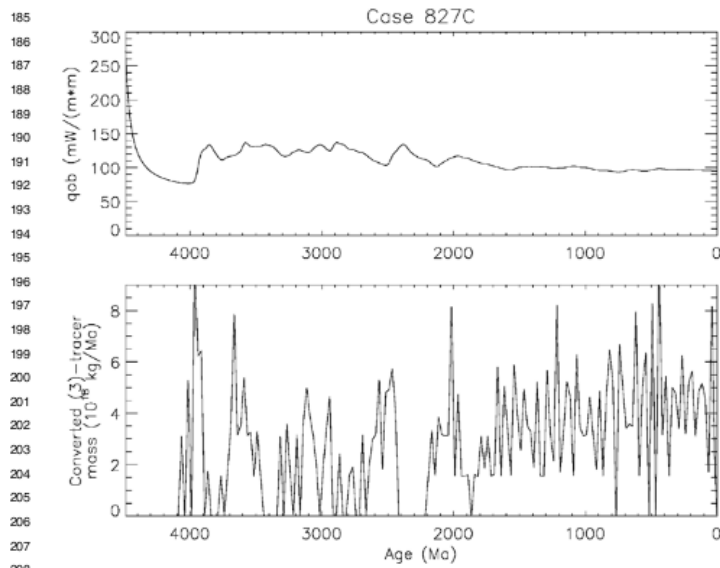
Fig. 2 The *upper panel* shows the evolution of the laterally averaged surface heat flow. The *lower panel* displays the episodic distribution of differentiation cycles of the juvenile contributions to the total mass of the continents. The rate of the converted continental-tracer mass has been averaged for every 25 Ma and plotted in discretized form. We converted the mass into units of 10^{18} kg/Ma. We used $\sigma_y = 110$ MPa and $r_n = -0.5$

T_{st} the initial temperature profile, T the temperature as a function of r, θ, ϕ and t. The quantity r_n is used for a stepwise shift of the viscosity profile from run to run in order to vary the temporally averaged Rayleigh number, Ra. After Yamazaki and Karato [27], $c = 14$ for $MgSiO_3$ perovskite and $c = 10$ for MgO wüstite. Therefore, the lower-mantle value for c should be somewhere between 10 and 14. For numerical reasons, we are restricted to a value of $c = 7$. For the uppermost 285 km of the mantle (including crust), we supplement (1) by a viscoplastic yield stress, σ_y:

$$\eta_{eff} = \min\left[\eta(P, T), \frac{\sigma_y}{2\dot{\varepsilon}}\right], \tag{2}$$

where P is pressure and $\dot{\varepsilon}$ is the second invariant of the strain-rate tensor. The devolatilization of oceanic lithosphere is expressed by a conventional high lithospheric viscosity in the profile $\eta_3(r)$. Plate-like behavior was generated by (2) and low asthenospheric viscosity [24].
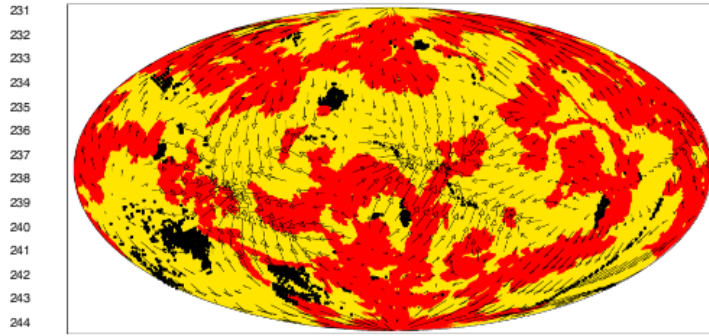
Run 827C   ys = 110 MPa   rn = −0.55   Merid. 180° midmost   Time = 4490 Ma
Age = −0.2775 Ma   Max vel = 1.923 cm/a   Av hor vel = 0.8056 cm/a

Fig. 3 The distribution of continents (*red*), oceanic plateaus (*black*), and oceanic lithospheric plates (*yellow*), covered by MORB crust, for the present. *Arrows* represent creep velocities. We used $\sigma_y = 110$ MPa and $r_n = -0.5$

Figure 3 shows a computed distribution of continents for the present. Of course, we are able to show such a kind of distribution for each time step. How realistic is this solution of our system of differential equations? To answer this question, we developed not only the computed continental distribution of the present day into spherical harmonics but also the *observed* distribution. The coefficients, A_n^m and B_n^m, depend not only on the distribution of continents but also on the position of the pole of the grid (θ, ϕ). Therefore, a direct comparison of the A_n^m and B_n^m of the two data sets makes no sense. For that reason, we computed an orientation-independent quantity, h_n^*, where h_n^* is a function of the A_n^m and B_n^m:

$$h_n^* = \frac{\sqrt{n \cdot (n+1)}}{2} \cdot \left\{ \sum_{m=0}^{n} [(A_n^m)^2 + (B_n^m)^2] \right\}^{1/2}. \tag{3}$$

The comparison of the h_n^*-n spectra is shown by Fig. 15 of Walzer et al. [25]. Using many cases, we found a realistic Ra-σ_y region.

3 Further Results: Predictable and Stochastic Features of the Model

Our convection-differentiation mechanism is partly predictable and partly stochastic. Essential features are predictable although the model as well as the real Earth show stochastic features at bifurcation points. The variable Rayleigh number, Ra_t, is

a function of time, essentially because of the temperature dependence of viscosity. The spatially averaged mantle viscosity increases since the Earth is cooling. This is essentially expressed by the second factor of the right hand side of (1). Therefore Ra_t decreases in the main part of the evolution time. But in some time intervals, we observe a Ra_t-growth due to feedback effects. Is it possible to predict the position of these individual rises on the time axis using the form of the Ra_t-curves of neighboring runs? Figure 4 presents a series of $Ra_t(t)$-evolutions for an equidistant succession of r_n-values. The yield stress, here called y_s, is kept constant. It is shown that the shift of the Ra_t-maxima is a nearly linear function of the viscosity-level parameter, r_n. So, these maxima are predictable for new neighboring runs between the presented ones. The average viscosity of the bottom panel of Fig. 4 is by a factor of about 0.7 lower than the average viscosity of the uppermost panel. Therefore the sequence of events is accelerated from the top to the bottom panel.

As a resolution test and in search of stochastic features, we performed each run twice with a differing number of tracers. We used about 10.5 million tracers for basic runs (B-runs) and about 84 million tracers for comparative runs (C-runs). In Fig. 5(a), we show a column of time evolutions of the variable Rayleigh number, Ra_t, for a fixed parameter r_n. The latter one mainly determines the level of the viscosity profile. The deviations between B-runs and C-runs seem to be mainly stochastic. The t-positions of the first three main maxima have a scarcely perceptible dependence on the viscoplastic yield stress. The corresponding features occur somewhat later for higher yield-stress values. Figures 5(b) and 5(c) show this weak dependence, too. However, a comparison of the prominent features of the curves *between* the columns in Fig. 5(a), 5(b), and 5(c) corroborates the strong dependence of the t-shift of the maxima of $Ra_t(t)$ on the viscosity-level parameter, r_n.

The panels of Fig. 6 display the juvenile additions to the total mass of the continents as a function of time, t, for the same variation of parameters as in Fig. 5. The first three groups of maxima of each run of Fig. 6 show partially predictable behavior, yet. In Fig. 6(a), the viscosity-level parameter is fixed at $r_n = -0.60$. The yield stress decreases in equidistant steps from $y_s = 135$ MPa for the top panel to $y_s = 115$ MPa for the bottom panel. The first group of peaks shows a very weak dependence on yield stress. The second peak group occurs about 40 Ma earlier in the bottom panel compared to the corresponding feature of the top panel. This is in accord with the results of Fig. 5. For the third group of maxima, we observe a slight shift in a similar order of magnitude. The distribution of later growth episodes is more or less non-correlated. Compared to the $Ra_t(t)$-curves, the course of chemical differentiation shows considerably higher portions of stochastic behavior. Similar conclusions can be found for Figs. 6(b) and 6(c). In Fig. 6(c), the second group of peaks of the bottom panel, for $y_s = 115$ MPa, occurs about 70 Ma earlier than the second group the top panel, for $y_s = 135$ MPa. The first group of maxima of the chemical differentiation in the third column (Fig. 6(c)) begins earlier than that of the first column (Fig. 6(a)) since the spatial average of viscosity is lower, independent of the variation of yield stress. This observation corresponds to the behavior of $Ra_t(t)$-curves. So, the evolution of differentiation of Fig. 6(c) is more rapid than that of 6(b) and even quicker than that of 6(a). This corresponds to the $Ra_t(t)$-behavior of Fig. 5.
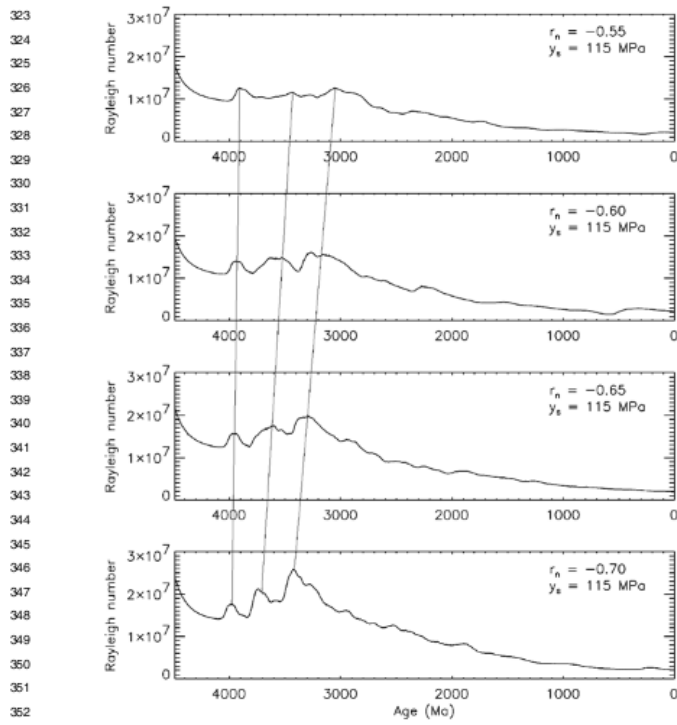
Fig. 4 A variation of the viscosity level parameter r_n. The time evolution of the variable Rayleigh number, Ra_t, of the cases show predictable shifts of prominent features as a function of r_n

To sum up it can be said that the evolution of the Rayleigh number is more predictable. The evolution of chemical differentiation of oceanic plateaus has also deterministic portions but it is considerably more stochastic than $Ra_t(t)$. Further conclusions can be found in the Abstract.

4 Numerical Method and Implementation

We use the code TERRA to model the thermal and chemical evolution of the Earth's mantle. The equations of momentum and energy balance are solved in a discretized spherical shell. The basic grid is defined by the corners of an icosahedron. By
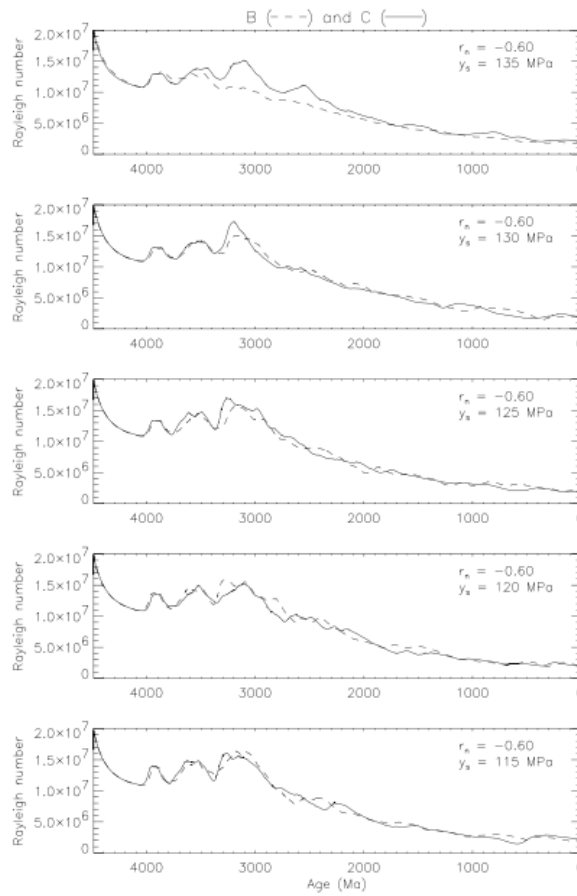
(a)

Fig. 5 The variable Rayleigh number, Ra_1, as a function of time. The present time is at the right-hand margin of the panels. In the first column, (**a**), the viscosity level parameter, r_n, is kept constant at -0.60, in the second column, (**b**), at -0.65, in the third column, (**c**), at -0.70. Within each column, the yield stress, y_s, varies from 135 MPa in the uppermost panel to 115 MPa in the bottom panel. *Dashed lines* signify B-runs, *solid lines* represent C-runs
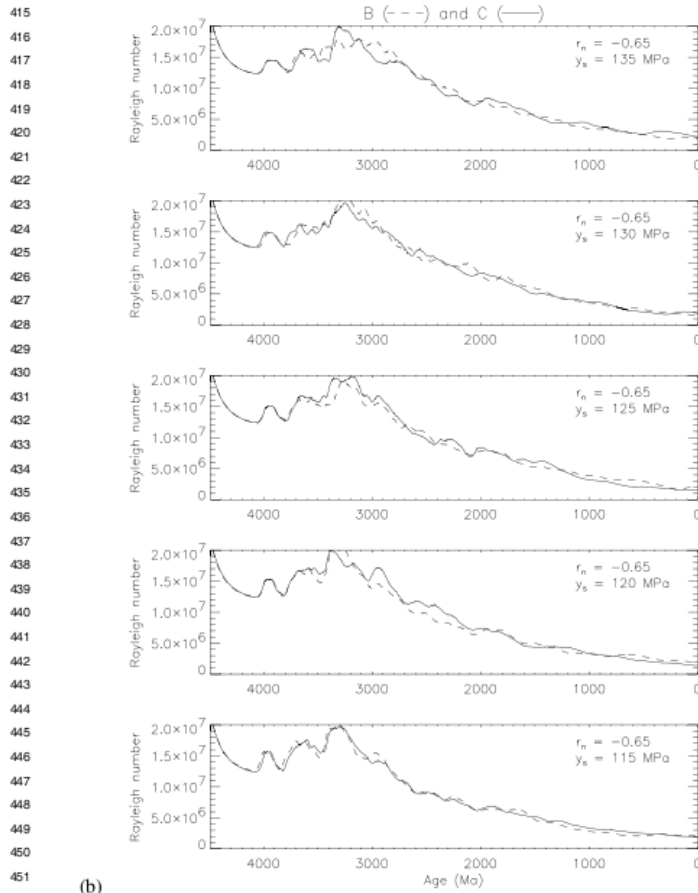
(b)

Fig. 5 (Continued)

dyadic subdivision of the icosahedron's edges and by projecting the resulting cor-
ners onto the spherical-shell surface we obtain an optionally refined grid in lateral
direction. Such grid-point distributions are concentrically repeated on additional in-
ternal spherical surfaces in almost regular distances in radial direction of the shell.
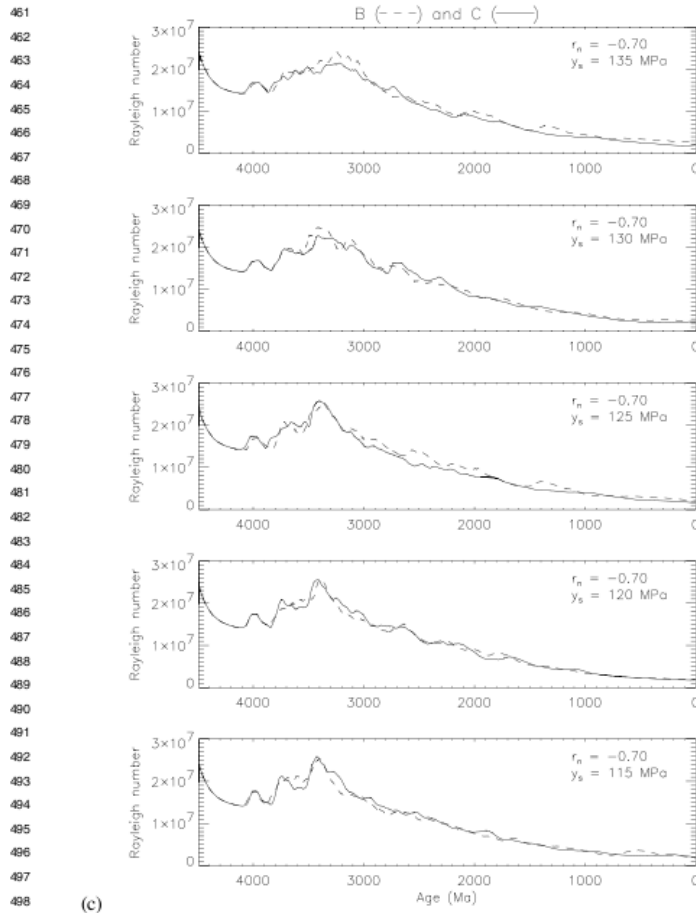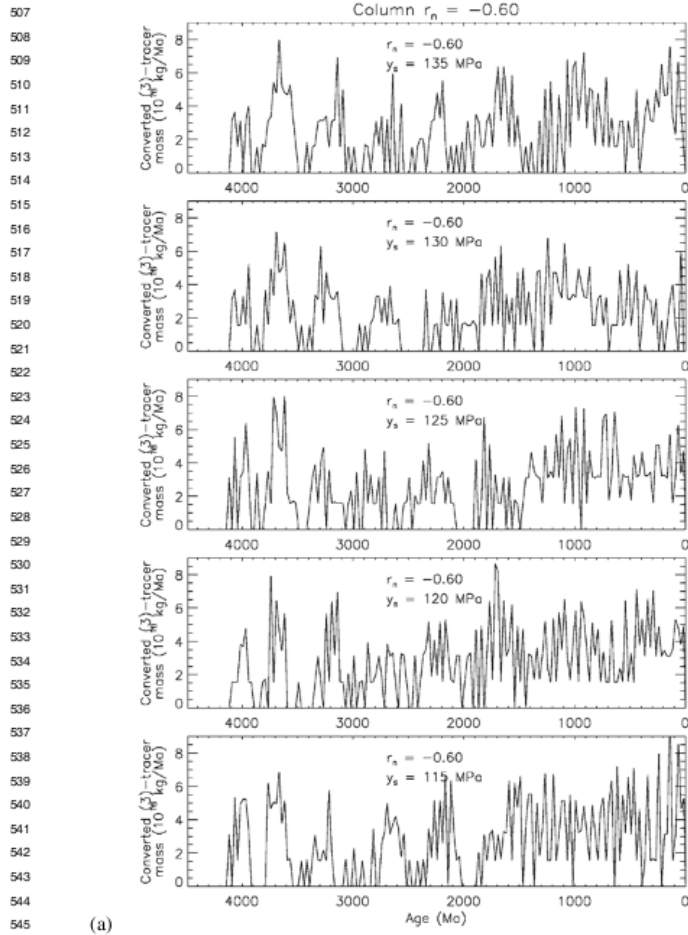
(c)

Fig. 5 (Continued)

For production runs we used 1,351,746 grid points. Stability test cases ran with 10,649,730 grid points.

The Navier-Stokes equations are handled by the Finite Element Method. Pressure and velocity are solved simultaneously by a Schur-complement conjugate-gradient

(a)

Fig. 6 The consequences of a variation of the parameters r_n and y_s for the evolution of the juvenile contributions to the total mass of the continents. The rate of the converted continental-tracer mass has been averaged for every 25 Ma and plotted in discretized form. We converted the mass into units of 10^{18} kg/Ma. The present time is at the right-hand margin of the panels. In the first column, (**a**), the viscosity level parameter, r_n, is kept constant at -0.60, in the second column, (**b**), at -0.65, and in the third column, (**c**), at -0.70. Within each column, the yield stress, y_s, varies from 135 MPa in the uppermost panel to 115 MPa in the *bottom panel*
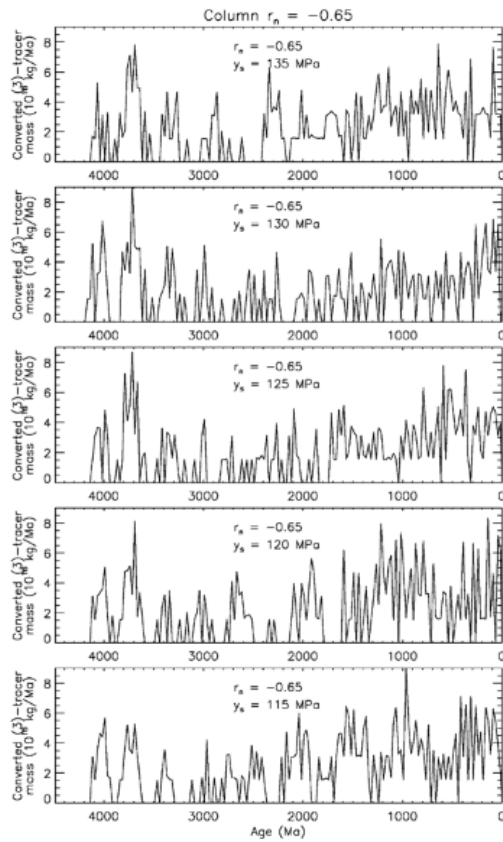
Fig. 6 (Continued)

iteration [20]. The system of linear equations is solved using a multigrid procedure in connection with matrix-dependent prolongation and restriction and with a Jacobi smoother. The temperature transport is realized by the second order Runge-Kutta method for explicit time steps.

For convergence tests we compared the results of runs with 1,351,746 and 10,649,730 nodes. The deviations concerning Rayleigh number, Nusselt number, Urey number, and the laterally averaged surface heat flow, qob, were smaller than
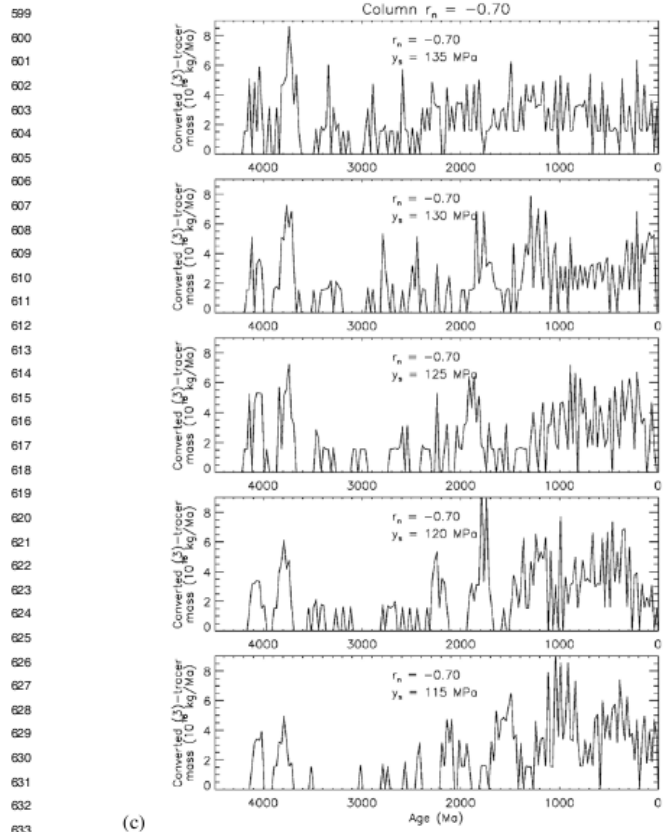
Fig. 6 (Continued)

The Terra code is parallelized by domain decomposition according to the dyadic grid refinement and using explicit message passing (MPI). In Table 1 we present measurements of scalability and performance. Using the performance measuring tool `jobperf`, we obtained an average of 1201 MFlop/s with 8 processors, 1116 MFlop/s with 32 processors, and 935 MFlop/s with 128 processors, respectively. In

Table 1 CPU-time, walltime and speedup for runs with 100 time steps on 1,351,746 nodes (a) and on 10,649,730 nodes (b). For comparison, Speedup (b) for 4 processors has been deliberately set to 4.00

Procs	CPU-time (a)	Walltime (a)	Speedup (a)	CPU-time (b)	Walltime (b)	Speedup (b)
1	00:27:13	00:27:17	1			
4	00:29:12	00:07:33	3.61	05:01:23	01:16:09	4.00
8	00:26:08	00:03:31	7.76	04:53:26	00:37:32	8.12
16	00:25:36	00:02:02	13.42	05:08:51	00:19:35	15.69
32	00:21:52	00:01:02	26.40	04:34:40	00:09:11	33.17
64				05:43:25	00:05:36	54.39
128				05:34:24	00:03:04	100.42

both resolutions the speedup was almost linear, in some cases slightly superlinear due to cache usage. With the high resolution, at least 4 processors are necessary to make efficient use of the cache memory.

References

1. D.H. Abbott, R. Drury, W.D. Mooney, Continents as lithological icebergs: The importance of buoyant lithospheric roots. Earth Planet. Sci. Lett. **149**, 15–27 (1997)
2. F. Albarède, The growth of continental crust. Tectonophysics **296**, 1–14 (1998)
3. R.J. Arculus, H. Lapierre, É. Jaillard, Geochemical window into subduction and accretion processes: Raspas metamorphic complex. Ecuador. Geol. **27**(6), 547–550 (1999)
4. V.C. Bennett, Compositional evolution of the mantle, in *Treatise on Geochemistry*, ed. by R.W. Carlson. The Mantle and the Core, vol. 2 (Elsevier, Amsterdam, 2003), pp. 493–519
5. M. Brown, T. Rushmer (eds.), *Evolution and Differentiation of the Continental Crust* (Cambridge Univ. Press, Cambridge, 2006)
6. H.P. Bunge, M.A. Richards, J.R. Baumgardner, A sensitivity study of three-dimensional spherical mantle convection at 10^8 Rayleigh number: Effects of depth-dependent viscosity, heating mode and an endothermic phase change. J. Geophys. Res. **102**, 11991–12007 (1997)
7. M.F. Coffin, O. Eldholm, Large igneous provinces: Crustal structure, dimensions and external consequences. Rev. Geophys. **32**, 1–36 (1994)
8. K.C. Condie, Episodic continental growth models: Afterthoughts and extensions. Tectonophysics **322**, 153–162 (2000)
9. J.P. Davidson, R.J. Arculus, The significance of Phanerozoic arc magmatism in generating continental crust, in *Evolution and Differentiation of the Continental Crust*, ed. by M. Brown, T. Rushmer (Cambridge University Press, Cambridge, 2006), pp. 135–172
10. R.V. Fisher, H.U. Schmincke, *Pyroclastic Rocks* (Springer, Berlin, 1984)
11. G.A. Glatzmaier, Numerical simulations of mantle convection: time-dependent, three-dimensional, compressible, spherical shell. Geophys. Astrophys. Fluid Dyn. **43**, 223–264 (1988)
12. G. Hirth, Protons lead the charge. Nature **443**, 927–928 (2006)

13. A.W. Hofmann, Chemical differentiation of the Earth: The relationship between mantle, continental crust and oceanic crust. Earth Planet. Sci. Lett. **90**, 297–314 (1988)

14. A.W. Hofmann, Sampling mantle heterogeneity through oceanic basalts: isotopes and trace elements, in *Treatise on Geochemistry*, ed. by R.W. Carlson. The Mantle and the Core, vol. 2 (Elsevier, Amsterdam, 2003), pp. 61–101

15. D.G. Howell, *Tectonics of Suspect Terranes: Mountain Building and Continental Growth* (Chapman and Hall, New York, 1989)

16. J.D. Kramers, I.N. Tolstikhin, Two terrestrial lead isotope paradoxes, forward transport modelling, core formation and the history of the continental crust. Chem. Geol. **139**, 75–110 (1997)

17. S. Mei, D.L. Kohlstedt, Influence of water on plastic deformation of olivine aggregates, 2: Dislocation creep regime. J. Geophys. Res. **105**(B9), 21,471–21,481 (2000)

18. T.F. Nagler, J.D. Kramers, Nd isotopic evolution of the upper mantle during the Precambrian: Models, data and the uncertainty of both. Precambrian Res. **91**, 233–253 (1998)

19. S.W. Parman, Helium isotopic evidence for episodic mantle melting and crustal growth. Nature **446**, 900–903 (2007)

20. A. Ramage, A.J. Wathen, Iterative solution techniques for the Stokes and the Navier-Stokes equations. Int. J. Numer. Methods Fluids **19**, 67–83 (1994)

21. G. Schubert, D.L. Turcotte, T.R. Olson, *Mantle Convection in the Earth and Planets* (Cambridge University Press, Cambridge, 2001)

22. A. Stracke, A.W. Hofmann, S.R. Hart, FOZO, HIMU and the rest of the mantle zoo. Geochem. Geophys. Geosys. **6**, Q05,007 (2005). doi:10.1029/2004GC000824

23. U. Walzer, R. Hendel, Mantle convection and evolution with growing continents. J. Geophys. Res. (2008 submitted)

24. U. Walzer, R. Hendel, J. Baumgardner, The effects of a variation of the radial viscosity profile on mantle evolution. Tectonophysics **384**, 55–90 (2004)

25. U. Walzer, R. Hendel, J. Baumgardner, Whole-mantle convection, continent generation, and preservation of geochemical heterogeneity, in *High Perf. Comp. Sci. Engng. '07*, ed. by W.E. Nagel, W. Jäger, M. Resch (Springer, Berlin, 2007), pp. 603–645

26. M. Willbold, A. Stracke, Trace element composition of mantle end-members: implications for recycling of oceanic and upper and lower continental crust. Geochem. Geophys. Geosys. **7**, Q04,004 (2006). doi:10.1029/2005GC001005

27. D. Yamazaki, S.I. Karato, Some mineral physics constraints on the rheology and geothermal structure of the Earth's lower mantle. Am. Min. **86**, 385–391 (2001)